Available online at www.sciencedirect.com
SCIENCE DIRECT®
PERGAMON
International Journal of Heat and Mass Transfer 46 (2003) 3337–3347
International Journal of HEAT and MASS TRANSFER
www.elsevier.com/locate/ijhmt

Study on heat driven pump. Part 2—Mathematical modeling

J.L. Xu, T.N. Wong *, X.Y. Huang

School of Mechanical and Production Engineering, Nanyang Technological University, Nanyang Avenue, Singapore 639798, Singapore

Received 26 September 2001; received in revised form 12 March 2003

Abstract

Literature shows that the study on heat driven pump mainly focused on the experimental aspect. Numerical modeling is scarce. In this paper a numerical model is proposed to simulate the thermal hydraulic characteristics of a heat driven pump based on a variable-node moving boundary formulation. In the two-phase region of the heat driven pump, homogeneous equilibrium flow is assumed. The governing equations are successfully integrated over the single-phases and two-phase time-dependent regions. The simulation results demonstrate that the working principle of the pump could be sub-divided into four distinct stages. Attempts have been made to compare the predictions with experimental data. The detailed thermal hydraulic characteristics, cycle behavior and factors affecting the pump performance are presented and discussed.

1. Introduction

A heat driven pump (Fig. 1) is a passive device which is capable of lifting liquid through the inlet check valve and discharging it through the outlet check valve as heat is supplied at the horizontal branch. The first generation of heat driven pump, with inside diameter of 11.5 mm and length of 1.0 m, was developed by Yamamoto et al. [1]. Due to its simplicity and reliability, it can be applied in miniature electronic cooling devices or fluid delivery system as report by Xu et al. [2]. Though the heat driven pump itself is a very simple piece of hardware, the flow within the device is very complex due to phase changes and interactions between the single-phase liquid and the two-phase mixture in dynamic respond to the opening and closure of check valves.

In view of the complexity of the flow, it is noted that the reported work in literature focused on the experiment and thermal performance of the devices [1]. No theoretical/numerical modeling was reported on its working principle. This paper attempts to develop a dynamic simulation model, applying the moving boundary technique, to simulate the thermal hydraulic characteristics of the heat driven pump. Comparison between the model predictions and experimental data will be presented and discussed.

2. Working principle

From the experimental observation reported in the previous paper by Xu et al. [2], the ideal working principle of the heat driven pump can be described as four distinct stages.

(a) Sensible heating (Fig. 1a);
(b) Phase change with single-phase liquid discharge (Fig. 1b);
(c) Two-phase blow down (Fig. 1c);
(d) Liquid suction from inlet check valve (Fig. 1d).

Initially the system is full of single-phase liquid and both the inlet and outlet valves are closed. During its operation, heat is supplied at the horizontal branch. Fluid temperature increases due to the sensible heating (Fig. 1a). The system pressure is slightly increased due to the volumetric expansion of the single-phase liquid and causes liquid discharge through the outlet check valve (Fig. 1a). This disturbance travels throughout the system at the sonic velocity within the single-phase liquid

* Corresponding author. Tel.: +65-6792-4062.
E-mail address: mtnwong@ntu.edu.sg (T.N. Wong).

0017-9310/03/$ - see front matter © 2003 Elsevier Science Ltd. All rights reserved.
doi:10.1016/S0017-9310(03)00143-1

Nomenclature

A	inside pipe area, m^2
A_0	orifice diameter of the check valve, m^2
C	sonic velocity of liquid, m/s
C_D	discharge coefficient of an orifice
C_P	heat capacity, J/kg °C
D	pipe inside diameter, m
f	refer to ρ, G, ρs
f	friction coefficient in the closure relationship section
$\bar{f}$	average valve of f in the ith node
g	gravity constant, 9.806 m/s^2
G	mass flux, kg/m^2s
i	any node point from 1 to j for the left liquid region, j to k for the two-phase region, and k to 1 for the right liquid region
K_L	pressure loss coefficient of the check valve, a variable relative to opening time
$K_{L,full}$	pressure loss coefficient of the check valve when the valve is full open
L_1	length of the vertical downcomer branch, m
L_2	length of the horizontal branch, m
L_3	length of the vertical riser branch, m
m	time-averaged discharge/suction mass flux, g/s
$\tilde{m}$	transient discharge flow rate, g/s
P	pressure, Pa or mm water
P_{air}	environment air pressure, Pa
P_h	inside perimeter of the pipe, m
Q	total heating power, W
q_w	actual heat flux in the inside surface of the horizontal branch, W/m^2
$q_{w,e}$	effect heat flux defined in Eq. (5), W/m^2
R	defined as in the body text
Re	Reynolds number
s	fluid entropy, J/kg K
t	time, s
T	temperature, K or °C
TT	cycle period, s
T_{in}	liquid temperature in the supply tank, °C
v_f	liquid specific volume, m^3/kg
v_{fg}	specific volume difference between the liquid and the vapor
V	velocity, m/s
x	vapor mass quality
z	axial coordinate, m
z_L	length of left liquid region, m
z_T	length from the check valve A inlet to the end of two-phase region, m
z_{total}	total length of the heat driven pump, m
α	void fraction
β	liquid volume expansion coefficient, 1/K
δ	coefficient in Eq. (12)
Φ_{f0}^2	two-phase frictional multiplier
γ, η, ζ	dimensionless parameters
μ	liquid viscosity, m^2/s
θ	inclination angle relative to the vertical position
ρ	densities, kg/m^3
ΔP_{crack}	crack pressure of the check valve, Pa
τ	opening time of check valve, s
τ_w	frictional pressure drop per unit length, Pa/m
Δt, Δz	time and length increment, s and m
$(\ )^*$	values at the previous time step
$(\tilde{\ })$	$\frac{d}{dt}(\ )$
$(\bar{\ })$	average value in the ith node

Subscripts

f	liquid
g	vapor
fg	values defined as gas minus liquid
i	values at the low boundary of node I
j	node at interface 1
k	node at interface 2

Superscripts

old	values at the previous time step
new	values at the present new time step

causing fluid pressure oscillation within the system. Since the discharged mass flow rate through the check valve is in respond to the small volumetric expansion of the liquid within the system, the discharge mass flow rate is very small. Any non-condensable gas dissolved in the system will flatten the pressure oscillation in this stage.

On the horizontal branch, continuous heat input at the wall triggers the nucleation boiling, which occurs when the bulk fluid is saturated. The flow within the heat driven pump is divided into three regions: single-phase liquid region (I), two-phase region and single-phase liquid region (II). The length of the two-phase region depends on the interfacial speed at interfaces 1 and 2 respectively and the mixture void fraction. Since both the inlet and outlet check valves are directional, interface 1 propagates leftward which ends at $Z_L = L_1$, whereas interface 2 moves rightward in the riser section causing liquid region (II) to discharge through the outlet check valve (Fig. 1b).

When interface 2 reaches the outlet check valve, two-phase blow down begins (Fig. 1c). During the blow down stage, the system experiences in a sudden depres-

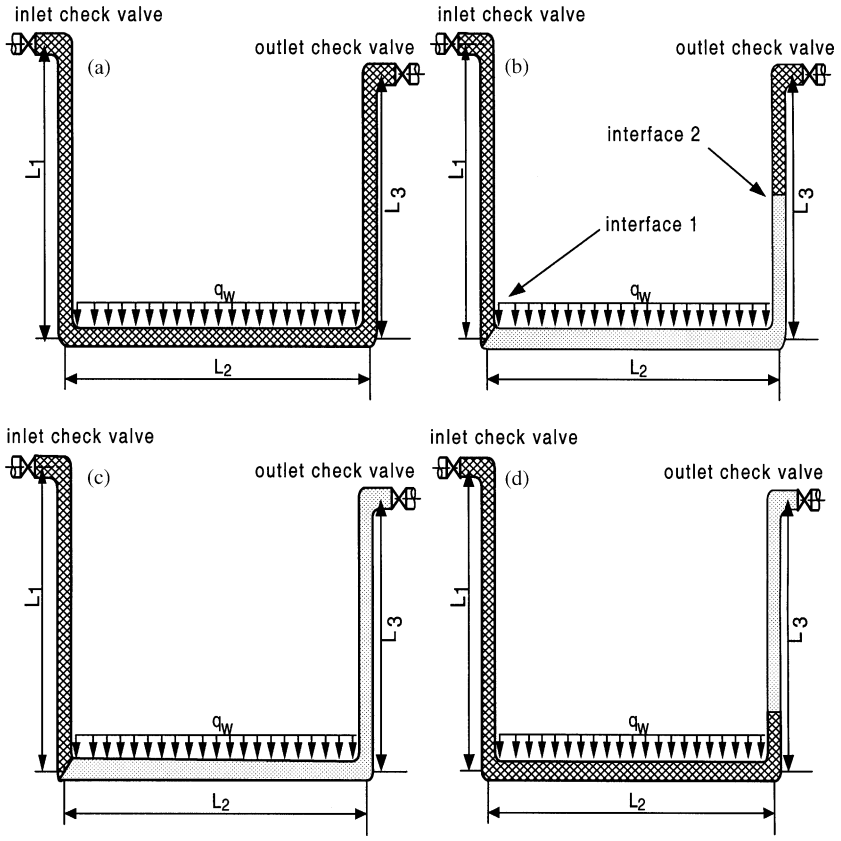

Fig. 1. The four typical stages of a full cycle in heat driven pump: (a) sensible heating stage; (b) phase change with liquid discharge; (c) two-phase blowdown and (d) liquid suction from inlet check valve.

surization. When the suction pressure, P_1, is low enough to overcome the crack pressure of the inlet check valve, the inlet check valve opens, which allows sub-cooled liquid to be sucked into the system (Fig. 1d). At this stage interface 1 propagates rightward in the horizontal branch and then in the riser section. The cycle repeats.

3. Theoretical modeling

The four distinct stages describing the working principle of the heat driven pump are modeled in detail as follows:

(a) Method of characteristics (MOC) formulation for single-phase sensible heating stage;
(b) Moving boundaries formulation to model the remaining three stages, i.e.:
  (i) Phase change in horizontal branch with single-phase liquid discharge stage,
  (ii) Two-phase blow down stage,
  (iii) Liquid suction from the inlet check valve.

3.1. Method of characteristic formulation in single-phase sensible heating stage

Conservation equations for one-dimensional flow of a non-conducting fluid are written as [3]:

Mass conservation equation

$$\frac{\partial P}{\partial t}+V\frac{\partial P}{\partial z}+\rho C^2\frac{\partial V}{\partial z}=\frac{\beta C^2}{C_P}\left[\frac{q_{w,e}P_h}{A}+\tau_w V\right] \tag{1}$$

Momentum conservation equation

$$\frac{\partial V}{\partial t}+V\frac{\partial V}{\partial z}+\frac{1}{\rho}\frac{\partial P}{\partial z}=-\frac{\tau_w}{\rho}-g\sin(\theta) \tag{2}$$

Energy conservation equation

$$\frac{\partial s}{\partial t}+V\frac{\partial s}{\partial z}=\frac{1}{\rho T}\left[\frac{q_{w,e}P_h}{A}+\tau_w V\right] \tag{3}$$

where $q_{w,e}$ and $\sin(\theta)$ are specified as

$$\sin(\theta)=\begin{cases}-1 & z\leqslant L_1\\ 0 & L_1<z\leqslant L_1+L_2\\ 1 & z>L_1+L_2\end{cases} \tag{4}$$

$$q_{w,e} = \begin{cases} q_w & L_1 < z < L_1 + L_2 \\ 0 & z < L_1 \text{ or } z > L_1 + L_2 \end{cases} \quad (5)$$

where β is the liquid volumetric expansion coefficient.

MOC solution approach is used to simulate the pressure wave oscillation within the system due to disturbance caused by liquid discharge and the on/off of the check valves. The computational procedure for obtaining P, V and s along the flow axis and time is described by Moody [3].

3.2. Moving boundaries formulation

Fig. 2 shows the schematic diagram for a heat driven pump model. The flow within the heat driven pump is divided into three regions: single-phase liquid region (I), two-phase region and single-phase liquid region (II). Because the interfaces 1 and 2 vary with time and there are large physical properties jump across the interface between the single-phase and two-phase mixture, the traditional finite difference method using the fixed node is not applicable to the present problem. A numerical approach with variable node moving boundaries developed by Constantine et al. [4] is incorporated into the model. The variable moving boundary model is described below.

3.2.1. The variable node system

Each region is divided into a number of nodes: e.g. from 1 to j for the liquid region (I), j to k for the two-phase region, and k to l for the liquid region (II), respectively. Each region's nodes have the same size. Define Z_L, Z_T, z_{total} as the distances measured from the inlet check valve. The non-dimensional lengths ζ, η, and γ for liquid region (I), two phase region and liquid region (II) are

$$\zeta = \frac{z}{z_L}, \quad \eta = \frac{z - z_L}{z_T - z_L}, \quad \gamma = \frac{z - z_T}{z_{total} - z_T}$$

where z is the distance measured from the inlet check valve. Since the same step size is applied in each region, hence

$$\zeta_{i+1} - \zeta_i = \text{constant}$$

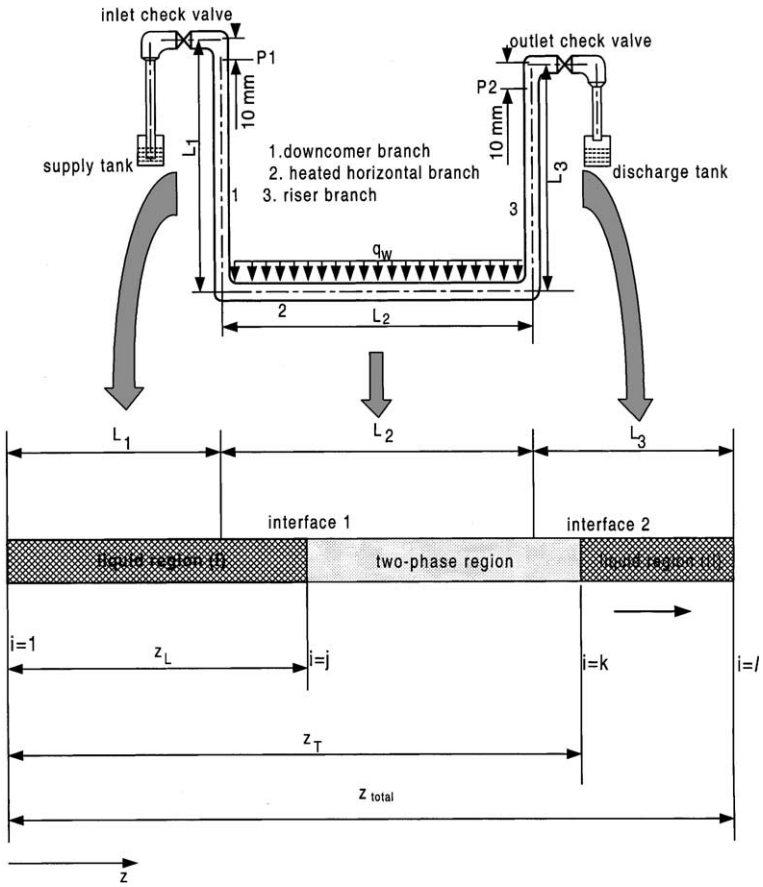

Fig. 2. One-dimensional coordinate system for the heat driven pump.

Table 1
Time derivative for z_i

	Liquid region (I)	Two-phase region	Liquid region (II)
z_i	$\zeta_i z_L$	$z_L + \eta_i(z_T - z_L)$	$z_T + \gamma_i(z_{total} - z_T)$
$\tilde{z}_i$	$\zeta_i \tilde{z}_L$	$\tilde{z}_L + \eta_i(\tilde{z}_T - \tilde{z}_L)$	$\tilde{z}_T - \gamma_i \tilde{z}_T$

$\eta_{i+1} - \eta_i = \text{constant}$

and

$\gamma_{i+1} - \gamma_i = \text{constant}$

The time derivatives $\tilde{\zeta}$, $\tilde{\eta}$ and $\tilde{\gamma}$ equal to zero. We define z_i as the distance of ith regional node from the inlet check valve, in each region z_i and its time derivative $\tilde{z}_i$ can be expressed in Table 1.

3.2.2. Conservation equations in the moving boundary stages

The conservation equations of mass, momentum and energy at a location z in the flow channel and at time t, for both single-phase liquid flow, and the homogeneous equilibrium two-phase mixture are [4]:

$$\frac{\partial \rho}{\partial t} + \frac{\partial G}{\partial z} = 0 \tag{6}$$

$$\frac{\partial G}{\partial t} + \frac{\partial}{\partial z}\left(\frac{G^2}{\rho}\right) + \frac{\partial P}{\partial z} = -\tau_w - \rho g \sin(\theta) \tag{7}$$

and

$$\frac{\partial(\rho s)}{\partial t} + \frac{\partial(Gs)}{\partial z} = \frac{1}{T}\left(\frac{q_{w,e} P_h}{A} + \tau_w V\right) \tag{8}$$

where $q_{w,e}$ and $\sin(\theta)$ are written in Eqs. (4) and (5). The energy equation is written in terms of the entropy. The first term of right side of Eq. (8) represents the entropy increase by the wall heating, while the second term represents the entropy increase by the work due to the wall shear stress (wall friction force). Compared with the wall heating effect, the entropy increase by the work due to the wall shear stress is very small and can be neglected.

In order to solve Eqs. (6)–(8), each region of the channel is subdivided into many nodes and these equations are integrated over the nodes. Since the node boundaries are changing versus time, the integrals that involve time derivatives are performed using the Leibnitz theorem to give

$$\int_{z_i}^{z_{i+1}} \frac{\partial f}{\partial t} \mathrm{d}z = \frac{\mathrm{d}}{\mathrm{d}t}\int_{z_i}^{z_{i+1}} f \,\mathrm{d}z - f_{i+1}\frac{\mathrm{d}z_{i+1}}{\mathrm{d}t} + f_i \frac{\mathrm{d}z_i}{\mathrm{d}t} \tag{9}$$

where

$f = \rho, G, \rho s$

$f_i = f(z_i, t)$

$f_{i+1} = f(z_{i+1}, t)$

$z_i, z_{i+1} = i$th node lower and upper boundary distance measured from the inlet check valve.

Since we have

$$\frac{\mathrm{d}}{\mathrm{d}t}\int_{z_i}^{z_{i+1}} f \,\mathrm{d}z = \frac{\mathrm{d}}{\mathrm{d}z}\left[\bar{f}_i(z_{i+1} - z_i)\right] \tag{10}$$

Eq. (9) yields

$$\int_{z_i}^{z_{i+1}} \frac{\partial f}{\partial t} \mathrm{d}z = \tilde{\bar{f}}_i \Delta z_i + \bar{f}_i(\tilde{z}_{i+1} - \tilde{z}_i) - f_{i+1}\tilde{z}_{i+1} + f_i \tilde{z}_i \tag{11}$$

where $\bar{f}_i$ average is the value of f_i in the ith node, $\tilde{} = \mathrm{d}/\mathrm{d}t$, $\Delta z_i = z_{i+1} - z_i$.

The average value $\bar{f}_i$ can be expressed as

$$\bar{f}_i = \delta f_i + (1 - \delta) f_{i+1} \tag{12}$$

δ has a range from 0.0 to 1.0 and its actual value relies on the shape of f_i in the ith node. For very small nodes, we can assume that f_i is linear within each node and $\delta = 0.5$ can be used. For larger nodes, $\delta = 0.5$ results in unstable and unmeaningful solutions. To avoid this problem, in the present work for the fluid flow in $+z$ direction, δ is set to be zero. Because the two check valves allow the flow in uni-direction, flow in $-z$ direction is not possible. Hence Eq. (11) is replaced by the following expression which is used in our calculation.

$$\int_{z_i}^{z_{i+1}} \frac{\partial f}{\partial t} \mathrm{d}z = \tilde{f}_{i+1} \Delta z_i - \tilde{z}_i \Delta f_i \tag{13}$$

where $\Delta f_i = f_{i+1} - f_i$.

The other terms that do not involve time derivatives in Eqs. (6)–(8) give

$$\int_{z_i}^{z_{i+1}} \frac{\partial G}{\partial z} \mathrm{d}z = G_{i+1} - G_i = \Delta G_i \tag{14}$$

$$\int_{z_i}^{z_{i+1}} \frac{\partial}{\partial z}\left(P + \frac{G^2}{\rho}\right)\mathrm{d}z = P_{i+1} - P_i + \left(\frac{G^2}{\rho}\right)_{i+1} - \left(\frac{G^2}{\rho}\right)_i = \Delta P_i + \Delta\left(\frac{G^2}{\rho}\right)_i \tag{15}$$

$$\int_{z_i}^{z_{i+1}} \frac{\partial(Gs)}{\partial z} \mathrm{d}z = (Gs)_{i+1} - (Gs)_i = \Delta(Gs)_i \tag{16}$$

In summary, the integration of Eqs. (6)–(8) over the variable node results in

$$\tilde{\rho}_{i+1} \Delta z_i - \tilde{z}_i \Delta \rho_i^* + G_{i+1} - G_i = 0 \tag{17}$$

$$\tilde{G}_{i+1}\Delta z_i - \tilde{z}_i \Delta G_i^* + \Delta\left(\frac{G^2}{\rho}\right)_i + P_{i+1} - P_i = -\int_{z_i}^{z_{i+1}} [\tau_w + \rho g \sin(\theta)]\,\mathrm{d}z \tag{18}$$

$$\frac{\partial(\rho s)_{i+1}}{\partial t}\Delta z_i - \tilde{z}_i \Delta(\rho s)_i^* + G_{i+1}s_{i+1} - G_i s_i = \int_{z_i}^{z_{i+1}} \frac{q_w P_h}{AT^*}\,\mathrm{d}z \tag{19}$$

where $*$ indicates values at the previous time step, note that values at the present time step has no such superscript.

The above three equations are applicable to both single-phase and two-phase regions. The additional derivatives for single-phase liquid in regions (I) and (II) and the two-phase region are described as follows in detail.

Single phase liquid in regions (I) and (II): In these regions, heating occurs only when $L_1 < z_i < L_1 + L_2$. Since liquid is assumed to be incompressible, Eq. (17) is not required. Eq. (19) is applied when $z_i > L_1$ and Eq. (18) describes the pressure distribution within the regions.

If the liquid temperature at interface 1 has achieved the saturated condition, the interface velocity at interface 1 can be obtained from Eq. (19) at the node $j-1$. The velocity of interface 1 is

$$\tilde{z}_L = \frac{\Delta\zeta z_L \rho_f \tilde{s}_f + \Delta(Gs)_{j-1}^* - \int_{z_{j-1}}^{z_j} \frac{q_w P_h}{AT^*}\,\mathrm{d}z}{\zeta_{j-1}\Delta(\rho s)_{j-1}^*} \tag{20}$$

Once the velocity at interface 1 is determined, the distribution of entropy for the region (I) can be calculated by substituting $\rho = \rho_f$ into Eq. (19) which gives

$$\tilde{s}_{i+1} = \frac{\tilde{z}_L \zeta_i \Delta(\rho s)_i^* - \Delta(Gs)_i^* + \int_{z_i}^{z_{i+1}} \frac{q_w P_h}{AT^*}\,\mathrm{d}z}{\rho_f \Delta z_i} \tag{21}$$

For the single-phase liquid region (II), since the flow is assumed to be adiabatic and incompressible, only Eq. (18) is considered. The interface velocity at interface 2 will be discussed in the next section.

Two-phase region: The flow is assumed to be homogeneous and in thermal equilibrium. The two-phase mixture density is defined as

$$\rho = \alpha\rho_g + (1-\alpha)\rho_f = \rho_f + \rho_{fg}\alpha \tag{22}$$

where α is the void fraction, $\rho_{fg} = \rho_g - \rho_f$. With the assumption that the influence of the small change of the pressure on the fluid properties can be neglected, the derivative of the density with time is

$$\tilde{\rho} = \rho_{fg}\tilde{\alpha} \tag{23}$$

The volumetric energy term (ρs) in Eq. (19) is defined as

$$\rho s = \alpha\rho_g s_g + (1-\alpha)\rho_f s_f \tag{24}$$

and

$$\frac{\partial(\rho s)}{\partial t} = R\tilde{\alpha} \tag{25}$$

where $R = \rho_g s_g - \rho_f s_f$.

Substituting Eqs. (22)–(25) into Eqs. (17) and (19) yields

$$\rho_{fg}\Delta z_i \tilde{\alpha}_{i+1} - \tilde{z}_i \Delta\rho_i^* + G_{i+1} - G_i = 0 \tag{26}$$

$$R\Delta z_i \tilde{\alpha}_{i+1} - \tilde{z}_i \Delta(\rho s)_i^* + G_{i+1}s_{i+1} - G_i s_i = \int_{z_i}^{z_{i+1}} \frac{q_w P_h}{AT^*}\,\mathrm{d}z \tag{27}$$

The boundary conditions on the interface 1 are

$$\begin{aligned} \alpha_j &= 0 \\ \rho_j &= \rho_f \\ G_j &= \rho_f \tilde{z}_L \\ s_j &= s_f \end{aligned} \tag{28}$$

The initial conditions at the beginning of the second stage (Fig. 1b) of the cycle for each nodes of the two-phase region are specified as

$$\begin{aligned} \alpha(t = t_B) &= 0 \\ \rho(t = t_B) &= \rho_f \\ G(t = t_B) &= \rho_f \tilde{z}_L \\ s(t = t_B) &= s_f \end{aligned} \tag{29}$$

where t_B is the time interval of the first stage of the cycle. For the first cycle, Eq. (29) is applicable to the whole horizontal length from $z = L_1$ to $z = L_1 + L_2$. For the following cycles, Eq. (29) is valid at $z = L_1 + L_2$, where the highest temperature is located.

Note that the integration of mass and energy conservation equations, Eqs. (26) and (27) are written in the implicit form to ensure stability of the iteration process. In the next time step, integration is performed from interface 1 to interface 2. Since the values at the previous time step $(\,)^*$ and the parameters on the lower boundary of the ith node at the present new time step $(\,)_i$ are known, Eqs. (26) and (27) involve the unknown parameters α_{i+1}, G_{i+1} and s_{i+1} at the new time step.

Entropy (s_{i+1}) is related to void fraction (α_{i+1}) by the following equations:

$$x_{i+1} = \frac{1}{1 + \frac{\rho_f}{\rho_g}\frac{1-\alpha_{i+1}}{\alpha_{i+1}}} \tag{30}$$

$$s_{i+1} = x_{i+1}s_g + (1 - x_{i+1})s_f \tag{31}$$

Eq. (26) is rewritten as

$$G_{i+1} = G_i - \rho_{fg}\Delta z_i \tilde{\alpha}_{i+1} + \tilde{z}_i \Delta\rho_i^* \tag{32}$$

A function with the void fraction of α_{i+1} in terms of Eq. (27) is defined as

$$f(\alpha_{i+1}) = R\,\Delta z_i \tilde{\alpha}_{i+1} + G_{i+1}s_{i+1} - \tilde{z}_i\,\Delta(\rho s)_i^* - G_i s_i - \int_{z_i}^{z_{i+1}} \frac{q_w P_h}{AT^*}\,\mathrm{d}z \tag{33}$$

When the integration is performed on the ith node, α_{i+1}, G_{i+1}, and s_{i+1} are the target variables to be pursed. Eq. (33) can be solved by Newton–Raphson iteration method

$$\alpha_{i+1}^{(\mathrm{new})} = \alpha_{i+1}^{(\mathrm{old})} - \frac{f\left[\alpha_{i+1}^{(\mathrm{old})}\right]}{f'\left[\alpha_{i+1}^{(\mathrm{old})}\right]} \tag{34}$$

where $f'(\alpha_{i+1})$ is the derivative function of $f(\alpha_{i+1})$ and can be computed as

$$f'(\alpha_{i+1}) = \frac{R\,\Delta z_i}{\Delta t} + s_{i+1}\frac{\partial G_{i+1}}{\partial \alpha_{i+1}} + G_{i+1}\frac{\partial s_{i+1}}{\partial \alpha_{i+1}} \tag{35}$$

where $\partial G_{i+1}/\partial\alpha_{i+1}$ and $\partial s_{i+1}/\partial\alpha_{i+1}$ can be derived from Eqs. (32) and (31), respectively.

$$\frac{\partial G_{i+1}}{\partial \alpha_{i+1}} = -\frac{\rho_{fg}\,\Delta z_i}{\Delta t} \tag{36}$$

$$\frac{\partial s_{i+1}}{\partial \alpha_{i+1}} = \frac{\partial s_{i+1}}{\partial x_{i+1}}\frac{\partial x_{i+1}}{\partial \alpha_{i+1}} = s_{fg}\frac{\rho_f \rho_g}{\rho^2} \tag{37}$$

where $s_{fg} = s_g - s_f$.

Once α_{i+1} is converged and G_{i+1} and s_{i+1} are determined, V_{i+1} is computed as

$$V_{i+1} = \frac{G_{i+1}}{\rho} \tag{38}$$

where ρ is the mixture density at the same location.

The velocity of interface 2 can be obtained from Eq. (38) at the upper boundary of node $k-1$.

Closure relationships: For the single-phase flow, τ_w, the shear stress per unit length in Eq. (18) is written as

$$\tau_w = f\frac{1}{D}\frac{G^2}{2\rho_f} \tag{39}$$

For two-phase flow, Eq. (39) shall be modified as

$$\tau_w = f\frac{1}{D}\frac{G^2}{2\rho_f}\phi_{f0}^2 \tag{40}$$

where f is the single-phase friction factor and is calculated as

$$f = \begin{cases} \frac{64}{Re} & Re < 2000 \\ \frac{0.3164}{Re^{0.25}} & Re > 2000 \end{cases} \tag{41}$$

$$Re = \frac{GD}{\mu_f} \tag{42}$$

ϕ_{f0}^2 is known as the two-phase frictional multiplier. In this work, a simple homogeneous model suggested by Collier [5] is used:

$$\phi_{f0}^2 = \left[1 + x\left(\frac{v_{fg}}{v_f}\right)\right]\left[1 + x\left(\frac{\mu_{fg}}{\mu_g}\right)\right]^{-0.25} \tag{43}$$

Check valve model: The inlet and outlet check valves allow the fluid to flow in uni-direction. The mass flow across the valves depends on pressure drop across the valve and the valve opening area. There are three assumptions used in the present model.

- The check valves open once the crack pressure is reached. The valves closed when the net pressure difference across the valve disappears.
- The time constant τ is defined as the opening time from the fully closed to fully open position.
- The check valves are modeled as orifices with a time-dependent pressure loss coefficient when the valve is in the opening transients.

Outlet check valve: Initially the valve is closed and the pressure difference across the valve is less than its crack pressure, hence

$$V_l = 0 \tag{44}$$

Once the pressure difference across the valve reaches its crack pressure, the valve opens and the pressure drop across the valve is

$$P_l - P_{air} = K_L\frac{\rho_f V_l^2}{2} \tag{45}$$

In Eqs. (44) and (45), P_l and V_l are the pressure and velocity at the end of the riser. K_L is the time-dependent pressure loss coefficient, defined as $K_L = K_{L,full}f(t,\tau)$. $f(\tau,t)$ is assumed to be

$$f(\tau,t) = \frac{K_L}{K_{L,full}} = \begin{cases} \frac{\tau}{t} & t < \tau \\ 1 & t \geqslant \tau \end{cases} \tag{46}$$

The above description is valid for single-phase liquid discharge. For two-phase mixture discharge through the valve, an orifice expression reported by Collier [5] is applied:

$$P_k - P_{air} = \frac{G_k^2 v_f}{2C_D^2}\left[\left(\frac{A}{A_0}\right)^2 - 1\right]\left[\frac{(1-x_k)^2}{1-\alpha_k} + \frac{v_g}{v_f}\frac{x_k^2}{\alpha_k}\right] \tag{47}$$

where x_k and α_k are defined at the upstream of the outlet check valve. A_0 is the orifice area. Define

$$K_L = \frac{1}{C_D^2}\left[\left(\frac{A}{A_0}\right)^2 - 1\right] \tag{48}$$

Eq. (47) is rewritten as

$$P_k - P_{air} = \frac{G_k^2 v_f K_L}{2}\left[\frac{(1-x_k)^2}{1-\alpha_k} + \frac{v_g}{v_f}\frac{x_k^2}{\alpha_k}\right] \tag{49}$$

Note that subscript "k" refers to the upper boundary of the two-phase region.

Inlet check valve: The pressure and suction velocity has the following relationship once the pressure difference attains its crack pressure as

$$P_{\text{air}} - P_1 = K_{\text{L}} \frac{\rho_{\text{f}} V_1^2}{2} \tag{50}$$

4. Solution method

In the above analysis, MOC solution approach is used to solve Eqs. (1)–(3) to simulate the compound pressure wave oscillation within the sub-cooled liquid due to disturbance caused by heat input, liquid discharge and the on/off of the inlet and outlet check valves. Once the saturated condition is reached at the horizontal branch, the flow is divided into single-phase and two-phase regions. Moving boundaries approach is employed to model the flow. Eqs. (20) and (21) are solved for single-phase region (I), whereas for the two-phase region, Eqs. (30)–(37) are computed until α_{i+1} is converged. The pressure distribution within the liquid regions (I and II) and two-phase region can be calculated by Eq. (18). The initial and boundary conditions at the two check valves have to be specified before the new time step calculation. After computing for one time step, the interface's positions 1 and 2 and the time derivative are updated. The same procedure is repeated for subsequent increment in the time step until the program ends.

5. Results and discussion

5.1. Comparisons of experimental results

To validate the mathematical model comparisons have been made with experimental results by Xu et al. [2]. The calculations were performed for the test section, with L_1 of 80 mm, L_2 of 80 mm, L_3 of 60 mm and the inner diameter of 3.0 mm. Because it is difficult to estimate the valve opening time τ, all the run cases were performed with $\tau = 10^{-5}$ s.

The time-averaged discharge and suction flow rates is integrated from the transient flow rate over a full cycle period as

$$m = \frac{\int_0^{\text{TT}} \tilde{m}\,\mathrm{d}t}{\text{TT}}$$

where TT is the cycle period and $\tilde{m}$ is the transient flow rate through the inlet/outlet check valve. Due to mass conservation in the device over a full cycle, the time-averaged suction mass flux is equal to that of discharge mass flux.

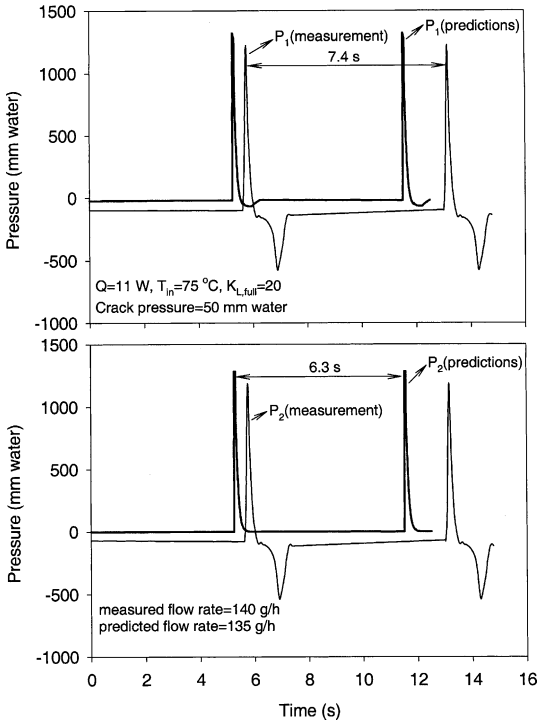

Fig. 3. Comparisons of pressures between predictions and experimental measurements.

Fig. 3 illustrates that the predicted P_1 and P_2 agree reasonably well with the measurements. The measured cycle period and the time-averaged flow rate are 7.4 s and 140 g/h respectively, and the predicted values are 6.3 s and 135 g/h respectively. Both the measurements and calculations illustrate the similar trend, with a smooth transition from the beginning of the new cycle to the onset of boiling taking place in the heating section, followed by the sharp pressure rising to a peak value, and a pressure falling stage. The measurements revealed that during the liquid suction stage, vacuum pressures (negative value) were always detected at both P_1 and P_2. This is due to the sub-cooled condensation between the saturated vapor and sub-cooled liquid. The sub-cooled condensation effect was not modeled in our calculations. The predicted negative pressure at P_1 is produced by the fluid density difference between the vertical downcomer and riser branch.

5.2. Cycle behavior

The predicted pulsating pressures, discharge and suction mass fluxes are presented in Fig. 4 with the same flow conditions as Fig. 3. The region A–B corresponds to the single-phase sensible heating stage. In this stage the high frequency pressure oscillations are solved by the present MOC calculations. However due to the small

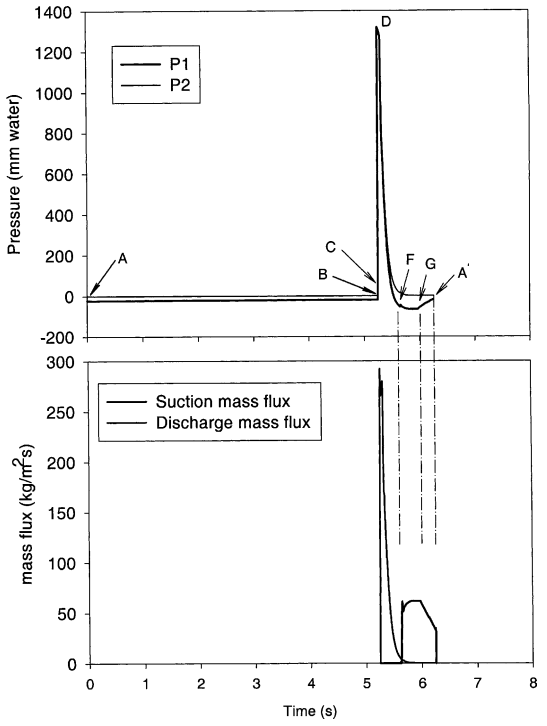

Fig. 4. Predicted transients of heat driven pump in one full cycle.

amount of non-condensable gas dissolved in the flow, the pressure oscillation was flatten with a slight pressure increased as shown in Fig. 3. Hence the average predicted pressure is plotted in Fig. 4 in this region. Region C–D indicates single-phase liquid discharge with boiling in the horizontal heating branch. It ends when interface 2 reaches the outlet check valve at time D. Due to the high liquid density, the discharge mass fluxes achieve a higher value for a short time lapse. Region D–F indicates the two-phase blow down stage. At the start of the two-phase blow down at time D, the pressure P_2 is considerably in excess of the atmosphere pressure, hence the system experiences a sudden depressurization. P_2 approaches the atmosphere pressure after a rapid pressure drops. The discharged two-phase mixture has a lower density, hence the discharge mass flux decreases. Due to the high void fraction in the vertical riser, the fluid density difference between the vertical riser and the vertical down-comer increases, as such vacuum pressure has attained at P_1. Liquid is induced into the system through the inlet check valve (region F–A). It is noted that the suction mass flux achieves its maximum value at $t = t_G$ which corresponds to the position of interface 1 located at the bottom of the vertical riser. Generally the characters from A to G have the same physical meaning which appeared in the previous paper in Fig. 2 by Xu et al. [2], and the predicted cycle behavior follows the findings by measurements by Xu et al. [2].

The present modeling results indicate of a two-phase blow down stage in the cycle. However, due to the subcooled condensation between the vapor and the subcooled liquid, the vapor may or may not reach the top of the vertical riser, depending on the heating power and the inlet liquid temperature in the supply tank [2].

5.3. Comparisons of heat driven pump performance

Fig. 5 shows comparison of cycle period and discharge flow rate between model predictions and measurements with an inlet liquid temperature of 80 °C. The results indicate that at lower heating power (<4 W) the cycle period decreases sharply with heating power, it approaches a constant value at higher heating power, which was confirmed by the measurements. The time-averaged discharge flow rate increases with heating power as expected.

When the heating power approaches the maximum value (about 14 W with inlet liquid temperature of 80 °C), very high void fractions and temperatures were predicted in the heating section. Under this condition, P_1 will not achieve vacuum pressure due to the high pressure in the system. The device loses its function beyond such upper-limit heating power.

Comparisons of predictions and measurements reveal that, large discrepancy occurs at lower heating power.

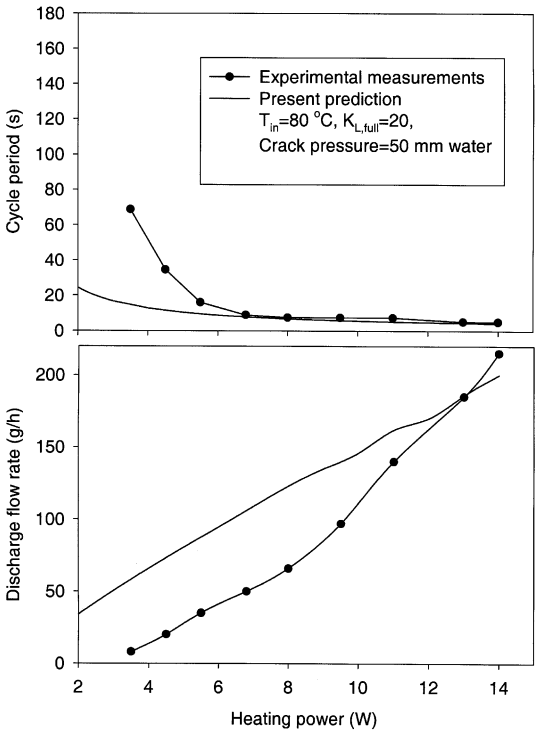

Fig. 5. Comparisons of heat driven pump performance between predictions and experimental measurements.

This is because it is difficult to estimate the corresponding heat loss to the environment at lower heating power, even though the heating section is well thermally insulated.

5.4. Effect of inlet liquid temperatures and check valve parameters

The effect of inlet liquid temperature on the heat driven pump performance is depicted in Fig. 6. It is seen that the cycle period decreases quasi-linearly with the liquid temperature. This is due to the fact that the single-phase liquid stage covers a large percentage of the cycle period, and the time for the sensible heating stage has a linear relationship with the inlet liquid temperature. Higher inlet liquid temperature result in the enhanced oscillating process thus higher flow rate is obtained.

Fig. 7 shows the cycle period and discharge flow rate versus pressure loss coefficient. It is demonstrated that

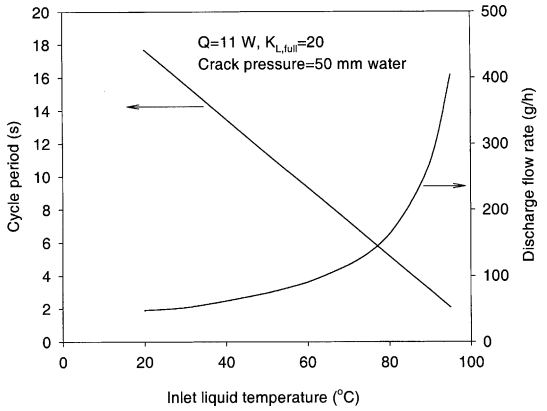

Fig. 6. Effect of inlet liquid temperature on the heat driven pump performance.

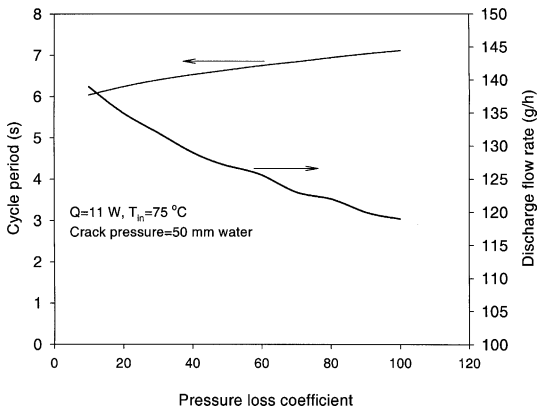

Fig. 7. Effect of pressure loss coefficients on the heat driven pump performance.

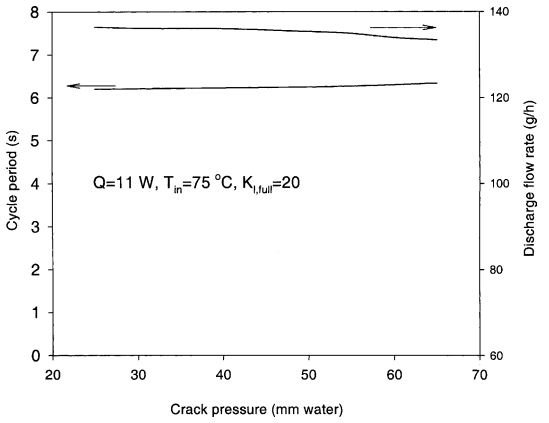

Fig. 8. Effect of crack pressure on the heat driven pump performance.

the cycle period increases with the pressure loss coefficient. Higher pressure drop coefficient will slow down a little bit of the oscillation process, hence the time-averaged discharge flow rate decreases.

It is interesting to note that the pump performance is insensitive to the crack pressures in the range from 25 to 65 mm water as show in Fig. 8. Referring to Fig. 4, the system pressure experiences a sudden pressure rise to a peak value once boiling is activated in the horizontal heating branch. Such pressure peak value is much higher than the crack pressure of the outlet check valve and the sudden pressure rise occurs in a very short time within the order of 1 ms. Therefore the crack pressure of the outlet check valve should have no influence on the pump performance. Similarly the crack pressure of the inlet check valve controls when the valve opens to suck the liquid. It also has little effect on the pump performance, but the crack pressure should be less than the maximum vacuum pressure that the system can create. Based on the present model, such maximum vacuum pressure is limited by the fluid density difference between the downcomer and the riser.

6. Conclusions

A dynamic model was developed to simulate the thermal hydraulic characteristics of a heat driven pump based on a variable-node moving boundary formulation. The simulation results demonstrated that the working principle of the pump could be subdivided into four distinct stages. These stages have also been confirmed by experimental observations. Comparison of the model prediction with experimental data can be reasonably accepted.

The simulated results show that the time-averaged discharge flows rate increases with heating power and

the cycle period approaches a constant value under higher heating power. Also the discharge flow rate increases with inlet liquid temperature. Both suction and discharge check valves maintain the flow in unidirectional and the valve characteristic has minimum influence on the pump performance.

Acknowledgements

This work is part of a research project on microscale cooling technology, which is financially supported by the National Science and Technology Board and the Ministry of Education of Singapore.

References

[1] T. Yamamoto, Y. Takamura, M. Katsuta, Study of Heat Driven Pump, J. Fuel Soc. Jpn. 59 (644) (1980) 1016–1024.
[2] J.L. Xu, X.Y. Huang, T.N. Wong, Study on heat driven pump. Part 1: Experimental measurement, Int. J. Heat Mass Transfer, in press, doi:10.1016/S0017-9310(03)00144-3.
[3] F.J. Moody, Introduction to Unsteady Thermofluid Mechanics, Wiley, New York, 1989.
[4] Constantine P. Tzanos, A movable boundary model for once-through steam generator analysis, Nucl. Technol. 82 (1988) 5–17.
[5] J.G. Collier, Convective Boiling and Condensation, McGraw-Hill, New York, 1981.